

P2X7 Receptors Trigger ATP Exocytosis and Modify Secretory Vesicle Dynamics in Neuroblastoma Cells^{*[5]}

Received for publication, April 29, 2010, and in revised form, January 31, 2011. Published, JBC Papers in Press, February 3, 2011, DOI 10.1074/jbc.M110.139410

Yolanda Gutiérrez-Martín^{‡S1}, Diego Bustillo^{‡S2}, Rosa Gómez-Villafuertes^{§¶2}, Jesús Sánchez-Nogueiro^{§¶1},
 Cristina Torregrosa-Hetland^{||}, Thomas Binz^{**}, Luis Miguel Gutiérrez^{||}, María Teresa Miras-Portugal^{§¶1},
 and Antonio R. Artalejo^{‡S3}

From the [‡]Departamento de Toxicología y Farmacología, [¶]Bioquímica y Biología Molecular, and [§]Instituto Universitario de Investigación en Neuroquímica, Universidad Complutense de Madrid, 28040 Madrid, Spain, the ^{||}Instituto de Neurociencias, Centro Mixto Consejo Superior de Investigaciones Científicas-Universidad Miguel Hernández, 03550 Sant Joan d'Alacant, Spain, and the ^{**}Institut für Biochemie, Medizinische Hochschule Hannover, 30625 Hannover, Germany

Previously, we reported that purinergic ionotropic P2X7 receptors negatively regulate neurite formation in Neuro-2a (N2a) mouse neuroblastoma cells through a Ca²⁺/calmodulin-dependent kinase II-related mechanism. In the present study we used this cell line to investigate a parallel though faster P2X7 receptor-mediated signaling pathway, namely Ca²⁺-regulated exocytosis. Selective activation of P2X7 receptors evoked exocytosis as assayed by high resolution membrane capacitance measurements. Using dual-wavelength total internal reflection microscopy, we have observed both the increase in near-membrane Ca²⁺ concentration and the exocytosis of fluorescently labeled vesicles in response to P2X7 receptor stimulation. Moreover, activation of P2X7 receptors also affects vesicle motion in the vertical and horizontal directions, thus, involving this receptor type in the control of early steps (docking and priming) of the secretory pathway. Immunocytochemical and RT-PCR experiments evidenced that N2a cells express the three neuronal SNAREs as well as vesicular nucleotide and monoamine (VMAT-1 and VMAT-2) transporters. Biochemical measurements indicated that ionomycin induced a significant release of ATP from N2a cells. Finally, P2X7 receptor stimulation and ionomycin increased the incidence of small transient inward currents, reminiscent of postsynaptic quantal events observed at synapses. Small transient inward currents were dependent on extracellular Ca²⁺ and were abolished by Brilliant Blue G, suggesting they were mediated by P2X7 receptors. Altogether, these results suggest the existence of a positive feedback mechanism mediated by P2X7 receptor-stimulated exocytotic release of ATP that would act on P2X7 receptors on the same or neighbor cells to further stimulate its own release and negatively control N2a cell differentiation.

Adenine nucleotides are well recognized extracellular signaling molecules mediating many physiological functions via the P2-type of purinergic receptors. P2 receptors are subdivided into ionotropic P2X and metabotropic P2Y subtypes (1). Up to now, seven mammalian P2X-receptor subtypes (P2X1–7) and eight mammalian P2Y-receptor subtypes (P2Y1, -2, -4, -6, -11, -12, -13, and -14) have been cloned and functionally characterized (2–4). P2X receptors are non-selective cation channels mediating Na⁺ and Ca²⁺ influx across the cell membrane, which leads to cell depolarization and the ensued activation of voltage-gated channels (5).

Purinergic signaling is already present at early stages of embryogenesis wherein it is involved in proliferation, migration, and differentiation of cells from multiple structures (6–9). Likewise, different purinergic receptors have been identified in a variety of both primary tumors and cell lines (10, 11). In this respect, recent data from our laboratory have shown that mouse neuroblastoma Neuro-2a cells (henceforth referred to as N2a⁴ cells) express ionotropic P2X7 receptors mediating cation currents that are selectively blocked by Brilliant Blue G (BBG) (12). As is also the case for hippocampal neurons (13), P2X7 receptors negatively regulate neurite formation in N2a cells through a Ca²⁺/calmodulin-dependent kinase II-related mechanism (12). Therefore, either by inhibiting P2X7 receptor activity with BBG or silencing its expression with shRNA, an increased neuritogenesis could be observed in N2a cell cultures. On the contrary, P2X7 receptor overexpression resulted in a significant reduction in the formation of neurites. These results imply the existence of an endogenous purinergic tone acting on P2X7 receptors to control neuronal differentiation of N2a cells. Interestingly, neuroblastoma cells are capable of releasing a variety of mediators including substance P and ATP itself (14, 15), and P2X7 receptor stimulation is also coupled to ATP release from human ACN neuroblastoma cells (16). Nevertheless, very little is known about the mechanisms involved in such a release process and, particularly, as to whether P2X7 receptors could be coupled to exocytosis from this sort of cells. In the

* This work was supported by Ministerio de Ciencia e Innovación Grants BFU2008-02699 and BFU2005-0634, Comunidad de Madrid Grant S-SAL-0253-2006, the Fundación Marcelino Botín, and "Spanish Ion Channel Initiative" (SICI) Grant CSD2008-00005.

⌘ Author's Choice—Final version full access.

[5] The on-line version of this article (available at <http://www.jbc.org>) contains supplemental Videos 1–5 and Figs. S1–S7.

¹ Supported by Comunidad de Madrid Postdoctoral Contract S-SAL-0253-2006.

² Supported by SICI.

³ To whom correspondence should be addressed: Dept. Toxicología y Farmacología, Facultad de Veterinaria, Universidad Complutense, Avda. Puerta de Hierro s/n, 28040 Madrid, Spain. Tel./Fax.: 34-91-394-3851; E-mail: antonio.artalejo@vet.ucm.es.

⁴ The abbreviations used are: N2a, Neuro-2a; BoNT/A, botulinum neurotoxin A; BBG, Brilliant Blue G; BzATP, 2',3'-O-(4-benzoyl)-benzoyl ATP; NEM, N-ethylmaleimide; STIC, small transient inward current; TIRFM, total internal reflection fluorescence microscopy; SNARE, soluble N-ethylmaleimide factor attachment protein (NSF) receptor; fF, femtofaraday; LDCV, large dense-core vesicle.

present study we have addressed this issue by identifying in N2a cells several essential proteins of the exocytotic apparatus of sympathetic neurons, including the vesicular catecholamine and nucleotide transporters, and by measuring exocytosis with both electrophysiological and imaging techniques in the presence of selective P2X7 receptor agents. Biochemical measurements based on the luciferin-luciferase reaction indicated that, in effect, N2a cells release ATP. Moreover, in clusters of N2a cells we report the detection of small transient inward currents (STICs), which are likely generated by the quantal release of ATP. Altogether, our results indicate that P2X7 receptors are coupled to exocytosis and to the regulation of secretory vesicle dynamics in N2a cells, and they suggest that the exocytotic release of ATP induced by P2X7 receptor stimulation could mediate the tonic inhibition of neurite formation exerted by P2X7 receptors in N2a cells.

EXPERIMENTAL PROCEDURES

Chemicals and Antibodies—2',3'-O-(4-Benzoyl)-benzoyl ATP (BzATP), BBG, ionomycin, bovine serum albumin, quinacrine, and *N*-ethylmaleimide (NEM) were purchased from Sigma. ARL 67156 was from Tocris Bioscience (Bristol, UK). Fura-2 AM, fluo-4 AM, rhod-2 AM, and Lysotracker red DND-99 were from Molecular Probes (Invitrogen). Botulinum neurotoxin A (BoNT/A) was purified as previously described (17).

Cell Culture—Murine Neuro-2a (ATCC® number CCL-131™) cells were cultured in Dulbecco modified Eagle's medium (Sigma) supplemented with Glutamax® (Invitrogen), penicillin/streptomycin (Invitrogen), and 10% heat-inactivated fetal bovine serum (EuroClone, Padova, Italy). Cells were grown at 37 °C in a humidified atmosphere containing 5% CO₂.

Electrophysiological Recordings—Electrophysiological recordings were performed with an EPC9 patch clamp amplifier using the PatchMaster software (HEKA Electronic, Lambrecht, Germany). Pipettes were pulled from Kimax borosilicate glass (Witz Scientific, Holland, OH) and subsequently wax-coated and fire-polished to obtain a final resistance of 2–3 megaohms when filled with standard solutions. The standard extracellular solution (Mg²⁺-free Locke's buffer) had the following composition: 140 mM NaCl, 4.7 mM KCl, 1.2 mM KH₂PO₄, 2.5 mM CaCl₂, 10 mM HEPES, and 5.5 mM glucose (pH 7.4, adjusted with NaOH; 294 mosM). External Ca²⁺-free solution had CaCl₂ replaced by 1 mM MgCl₂. Recording pipettes were filled with a solution containing 140 mM KCl, 1 mM MgCl₂, and 10 mM HEPES (pH 7.2, adjusted with KOH; 290 mosM). Cells attached to glass coverslips (10⁴ cells/ml) were transferred to a recording chamber placed on the stage of an inverted Zeiss Axiovert 100 microscope and continuously superfused with Locke's buffer (perfusion rate of 1 ml min⁻¹). Membrane currents were measured in the whole-cell configuration of the patch clamp technique (18), filtered at 2 kHz, and sampled at 10 kHz. Series resistance was compensated by 80% and monitored throughout the experiment together with the cell membrane capacitance. STICs were analyzed off-line using PatchMaster to calculate peak amplitude, rise time (20–80% of the peak amplitude), and half-decay time (to 50% of peak amplitude). Such events were detected using amplitude threshold set to 3 times the S.D. of the

noise, and each of them was visually inspected and additionally filtered to avoid artifactual noise components.

Exocytosis was estimated by the membrane capacitance increment according to the Lindau-Neher technique implemented as the "Sine + D" feature of the PatchMaster lock-in module (19, 20). A 1-kHz, 70-mV peak-to-peak amplitude sinusoidal function was superimposed onto the holding voltage (V_h ; -70 mV). To determine the change in capacitance values, membrane capacitance was first averaged over 2 s preceding purinergic agonist (BzATP) or plain Locke's solution application to give a base-line value; this was subtracted from the value estimated after drug or saline administration averaged over a 10-s window, excluding the first 1 s to avoid contamination by nonsecretory capacitative or purinergic currents. Experiments were performed at room temperature (22–24 °C).

Modified solutions and drugs were applied onto the cell under investigation by means of a gravity-driven perfusion system with 5 independent lines controlled by electronic valves (The Lee Co., Westbrook, CO). This system allowed the exchange of the medium surrounding a cell in less than 200 ms. In experiments involving the recording of STICs, drugs were locally applied by pressure ejection from a patch-pipette (2–5 μm tip diameter) placed few μm away from a cell cluster. Pressure pulses were delivered by an electronically controlled air pump (MPCU, List Electronic, Darmstadt, Germany) at low amplitudes (5–10 cm H₂O) to reduce bulk movement of the extracellular fluid. Stock solutions of drugs were diluted daily in extracellular saline and incorporated into the perfusion system a few minutes before starting the experiments.

Total Internal Reflection Fluorescence Microscopy (TIRFM) Studies of Vesicle Fusion and Motion—The TIRF system was based on a IX81 microscope (Olympus) equipped with a 100×, 1.45 NA, Plan Apochromat Olympus objective (pixel size, 80 nm). Two laser beams emitting at 488 and 561 nm were used to alternately illuminate the cell footprint, and the corresponding fluorescence signals were band-pass-filtered with a dual-band (emission between 500–550 nm and 580–620 nm) filter (Chroma Technology Corp., Rockingham, VT). A filter wheel-based epifluorescence illumination system (MT20; Olympus) was also coupled to the setup by using an Olympus TIRFM IX2-RFACA attachment system. Imaging was performed with a C9100 EM-CCD digital camera from Hamamatsu (Hamamatsu) controlled by CellR software (Olympus). Separated images corresponding to each of the laser illumination sources were acquired at a rate of 20 Hz to detect vesicle fusion or 1 Hz to monitor vesicle motion. Exposure time was 10 and 50 ms, respectively. TIRFM calibration was performed according to Wu *et al.* (21), and decay constant of the evanescent field (1/e depth) was determined to be 160 ± 28 nm.

Different combinations of fluorescent dyes were used to label the cells. In experiments aimed at simultaneously determining vesicle fusion and the intracellular calcium concentration ([Ca²⁺]_i), N2a cells plated on coverslips inside 35-mm cell culture dishes (2.5 × 10⁵ cells/dish) were loaded with quinacrine (2 μM; excited by 488-nm light) and rhod-2 AM (10 μM; excited by 561-nm light) for 20 min at 37 °C. At variance, N2a cells were incubated with Lysotracker red (2 μM; excited by 561-nm light) and fluo-4 AM (10 μM; excited by 488 nm light) in experiments

P2X7 Receptor-mediated ATP Exocytosis in Neuroblastoma Cells

designed to monitor vesicular motion as well as $[Ca^{2+}]_i$. Fusion of a vesicle and release of its content into the extracellular space was detected as a rapid loss of the quinacrine signal (in less than 500 ms). During the experiments, cells were continuously superfused with Locke's medium at a rate of 1.5 ml min^{-1} , and P2X7 receptor-selective agents were applied by bath superfusion. Perfusion was gravity-driven, and solution exchange was performed by manually operating the electronic valves of a VC-6 drug application system (Warner Instruments). Experiments were performed at 37°C .

Images were processed using the ImageJ software (public domain image processing program developed by Wayne Rasband at the National Institutes of Health, Bethesda, Maryland) with plug-ins for image average, region of interest measurements, and particle centroid tracking. Further analysis such as determination of mean square displacement according to Qian *et al.* (22) and z distances according to Johns *et al.* (23) were performed using homemade macros for IgorPro (WaveMetrics Inc., Lake Oswego, OR). $[Ca^{2+}]_i$ -related signals are presented as relative fluorescent intensities (F/F_0) rather than absolute concentrations.

Luciferin-Luciferase Luminescence Assay—Extracellular ATP concentration was measured using ENLITEN® rLuciferase/Luciferin reagent (Promega, Madison, WI). N2a cells were grown in 6-well plates till confluence. Culture medium ($100 \mu\text{l}$) was collected under various experimental conditions and centrifuged at $600 \times g$ for 5 min at 4°C , and $10\text{-}\mu\text{l}$ aliquots of supernatant were transferred to wells of a 96-well plate placed on ice. The 96-well plate was set in a FLUOstar OPTIMA Microplate Luminometer (BMG LABTECH GmbH, Offenburg, Germany), and $100 \mu\text{l}$ of rLuciferase/Luciferin reagent was automatically injected into each well at room temperature ($\sim 25^\circ\text{C}$). Immediately before the start of the experiments, N2a cells were bathed in Mg^{2+} -free Locke's buffer for 1 h at 37°C . Then cells were exposed for 5 min to either plain extracellular Locke's buffer or Locke's buffer supplemented with $100 \mu\text{M}$ ARL 67156, a competitive inhibitor of ecto-ATPases (24), with $500 \mu\text{M}$ NEM or with the two compounds, and their medium was collected to measure basal ATP concentration. Thereafter, cells were stimulated by adding ionomycin ($10 \mu\text{M}$, final concentration in extracellular medium) prepared in either plain Locke's buffer or Locke's buffer containing the above-mentioned supplements. Five minutes later, extracellular medium was again collected to measure evoked ATP concentration. In another set of experiments, cells were grown for 72 h in the absence or the presence of BoNT/A (30 nM). Both controls and toxin-treated cells were incubated with ARL 67156 ($100 \mu\text{M}$; 5 min) and subsequently challenged with ionomycin ($10 \mu\text{M}$; 5 min) to elicit ATP release. ATP concentration was determined by comparison with a calibration curve generated with ATP standards diluted in the same buffer as the samples.

Data Analysis—Pooled data are shown as the means \pm S.E.; n denotes the number of individual cells, vesicles, exocytotic events, or STICs considered in each particular analysis. Statistical differences were determined by the Student's t test for unpaired samples. A p value equal or smaller than 0.05 was taken as the limit of significance.

RESULTS

P2X7 Receptors Trigger Exocytosis as Assayed by Membrane Capacitance Measurements—It has been reported that N2a cells transiently transfected with pro-opiomelanocortin undergo calcium-regulated release of β -endorphin located to dense-core granules (25, 26). On the other hand, N2a cells express ionotropic purinergic P2X7 receptors whose activation promotes Ca^{2+} entry into the cell and the ensued increase in $[Ca^{2+}]_i$ (12). Thus, the question arises as to whether P2X7 receptors might be coupled to exocytosis in this neuroblastoma cell line. We first addressed this issue by determining the potential change in membrane capacitance elicited by P2X7 receptor stimulation. Biological membranes behave as electrical capacitors whose capacitance is in direct relation to their surface. Because exocytosis involves the fusion of the vesicle membrane with the plasma membrane, it implies an increase in cellular surface, which can be detected as a change in the capacitance of the cell by using the whole-cell configuration of the patch clamp technique (20, 27). In these experiments we employed N2a cells seeded at a low density (10^4 cells/ml) and systematically chose cells with a rounded shape and isolated from neighbors (Fig. 1A). Resting membrane capacitance of N2a cells was 10.03 ± 0.33 picofarads ($n = 19$). Selective activation of P2X7 receptors with BzATP ($100 \mu\text{M}$ for 10 s) induced inwardly directed non-desensitizing currents that were consistently associated with an increase in membrane capacitance (Fig. 1B). The mean charge of the currents evoked by BzATP was 93.15 ± 25.47 picocoulombs, and the capacitance increase was 84.77 ± 9.46 femtofarads ($n = 9$ cells) (Fig. 1, B and C). None of these effects could be due to an application artifact, as perfusing Locke's solution during 10 s did not cause any consistent change in whole-cell current and was associated to a capacitance increase of only 2.5 ± 2.5 femtofarads ($n = 5$ cells). On the contrary, it can be attributed to the activation of P2X7 receptors, as treatment with BBG ($5 \mu\text{M}$, 3 min before and during agonist application), a selective P2X7 receptor antagonist (28), reduced the currents (12.58 ± 2.94 picocoulombs) and the capacitance increase (22.2 ± 12.23 femtofarads) evoked by BzATP by 85 and 73%, respectively ($n = 5$ cells) (Fig. 1, B and C). Calcium-dependent neuroexocytosis requires the formation of the SNARE (soluble N -ethylmaleimide-sensitive fusion protein (NSF) attachment protein receptor) membrane fusion complex between two plasma membrane proteins, syntaxin and SNAP-25, and one vesicular protein, synaptobrevin/VAMP (29). SNARE complexes are disassembled due to the ATPase activity of NSF, which allows recovery of the components of the fusion complex for subsequent rounds of exocytosis (30). Accordingly, NEM has been used as tool to inhibit vesicle fusion underlying the exocytosis of a variety of mediators including ATP (31). Interestingly, treatment of N2a cells with $500 \mu\text{M}$ NEM for 2 min abolished the capacitance increase elicited by BzATP without reducing P2X7 receptor-mediated currents (supplemental Fig. S1). Altogether, these results indicate that P2X7 receptors are coupled to exocytosis in N2a cells.

P2X7 Receptors Trigger Exocytosis as Assayed by TIRFM Imaging—To corroborate electrophysiological results, we employed TIRFM to visualize exocytosis of individual large

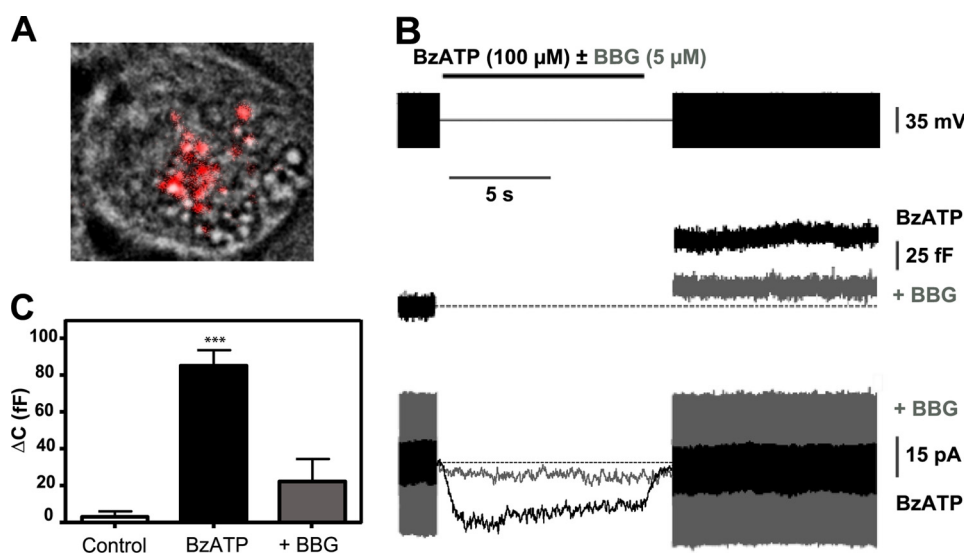


FIGURE 1. P2X7 receptor stimulation triggers exocytosis from N2a cells. *A*, superimposed images of an N2a cell loaded with LysoTracker red visualized using bright field and TIRF microscopy are shown. Note the rounded shape of the cell and the granular appearance of its cytoplasm under differential interference contrast optics; the fluorescence image shows LysoTracker red-labeled vesicles located in a ≈ 200 -nm thin layer of cytosol adjacent to the plasma membrane in contact with the glass coverslip ("footprint"). *B*, a patch clamp recording of whole-cell currents (*lower panel*) and membrane capacitance changes (*middle panel*) induced by BzATP ($100 \mu\text{M}$, 10 s; BzATP) in the absence and the presence of BBG ($5 \mu\text{M}$; +BBG) in a N2a cell is shown. BBG was administered 3 min before and during BzATP application. *Dashed lines* indicate membrane capacitance before stimulation and a zero current level, respectively. Current responses to a voltage sine wave (1-Hz, 70-mV peak to peak; *black boxes* in the voltage protocol shown in the *upper panel*) were used to estimate membrane capacitance. $V_h = -70$ mV. *C*, capacitance changes evoked by BzATP in the absence (BzATP; $n = 9$ cells) and the presence of BBG (+BBG; $n = 5$ cells) in N2a cells are shown. The *control bar* depicts the capacitance response to Locke's superfusion in a different set of cells ($n = 5$ cells). ***, $p < 0.005$ with respect to control.

dense-core vesicles (LDCVs) from N2a cells. In TIRFM only a thin layer close to the coverslip glass-solution interface is excited by the evanescent field generated by total reflection of the incident light, endowing this sort of microscopy with an extraordinary sensitivity to detect membrane-proximal fluorescent molecules. We made use of quinacrine, an acidophilic dye that binds ATP in catecholaminergic and peptidergic vesicles (32–34), and rhod-2, a Ca^{2+} indicator dye, to image single-vesicle exocytosis and $[\text{Ca}^{2+}]_i$ after activation of P2X7 receptors. LDCVs appeared as diffraction-limited fluorescent spots in the evanescent field whose penetration depth (decay constant of ≈ 160 nm) ensured that only labeled vesicles that are close to the cell membrane adhering to the coverslip are visualized. The number of quinacrine-labeled vesicles per N2a cell footprint was 8.03 ± 1.94 , which implies an average density of 0.082 ± 0.021 vesicles/ μm^2 ($n = 120$ cells). BzATP ($100 \mu\text{M}$, 30 s) administration was followed by an increase in rhod-2 fluorescence and a reduction in the number of quinacrine fluorescence spots (Fig. 2, A–D; see [supplemental Videos S1 and S2](#)). We could not resolve short-lived bright submicrometer spots of near membrane rhod-2 fluorescence, characteristic of local $[\text{Ca}^{2+}]_i$ elevations (35). The fluorescence signal averaged over the entire footprint reflected a slow but transient increase of $[\text{Ca}^{2+}]_i$ very much like that observed when epifluorescence measurements of global cytosolic Ca^{2+} are performed in N2a cells loaded with the ratiometric dye fura-2 AM (see [supplemental Video S3 and Fig. S2](#)). A rough estimate of $[\text{Ca}^{2+}]_i$ can be obtained from the K_d of rhod-2 (570 nm), the saturating ratio $R_{\text{max}} = \Delta F/F_{\text{max}}$, and the resting $[\text{Ca}^{2+}]_i$ (36). Post-stimulation values were in the range of 0.2–1 μM and were consistent with those obtained from fura-2 measurements using similar stimulation conditions ($0.41 \mu\text{M} \pm 0.09$; $n = 141$ cells; see [supplemental Fig. S2](#)). As expected for a Ca^{2+} -regulated process, exo-

cytosis of quinacrine occurred in parallel with the elevation of $[\text{Ca}^{2+}]_i$ ([supplemental Fig. S3](#)).

It is worth noticing that Locke's superfusion of the cells was not associated to a change in $[\text{Ca}^{2+}]_i$ (data not shown), whereas the occurrence of spontaneous exocytotic events was fairly rare. Moreover, adding BBG ($5 \mu\text{M}$) to the perfusion saline 5 min before and during BzATP application blunted the $[\text{Ca}^{2+}]_i$ response to the P2X7 receptor agonist and markedly reduced the probability of observing exocytotic events. We expressed the frequency of exocytotic events under the different experimental conditions as the fraction (%) of quinacrine fluorescence spots that were lost over a time window of 50 s after a change in the perfusion medium. As it is depicted in Fig. 2E, the frequency of spontaneous exocytotic events was $3.17 \pm 1.1\%$ ($n = 48$ cells), a value that increased three times upon BzATP administration ($10.29 \pm 2.3\%$; $p < 0.01$; $n = 52$ cells). Furthermore, in the presence BBG, the fraction of exocytotic events was diminished to $3.12 \pm 2.0\%$ ($n = 20$ cells), a figure not significantly different from that observed in non-stimulated cells. Interestingly, in cells treated with NEM ($500 \mu\text{M}$ for 2 min), the frequency of exocytosis after BzATP application was also reduced to control levels ($2.988 \pm 0.85\%$; $n = 36$ cells; data not shown). Likewise, BoNT/A (30 nM for 72 h), a *Clostridium* toxin with endopeptidase activity against SNAP-25 (37), reduced the percentage of quinacrine events from 10.44% ($n = 48$ cells) to 4.2% ($n = 44$ cells), an effect accompanied by the cleavage of SNAP-25 as determined by Western blot ([supplemental Fig. S4](#)). Thus, TIRFM imaging confirms previous electrophysiological data involving P2X7 receptors in exocytosis from N2a cells.

P2X7 Receptors Control LDCV Mobility at the Subplasmalemma Region— Ca^{2+} -dependent exocytosis of secretory vesicles is the result of a cascade of events comprising the anchoring

P2X7 Receptor-mediated ATP Exocytosis in Neuroblastoma Cells

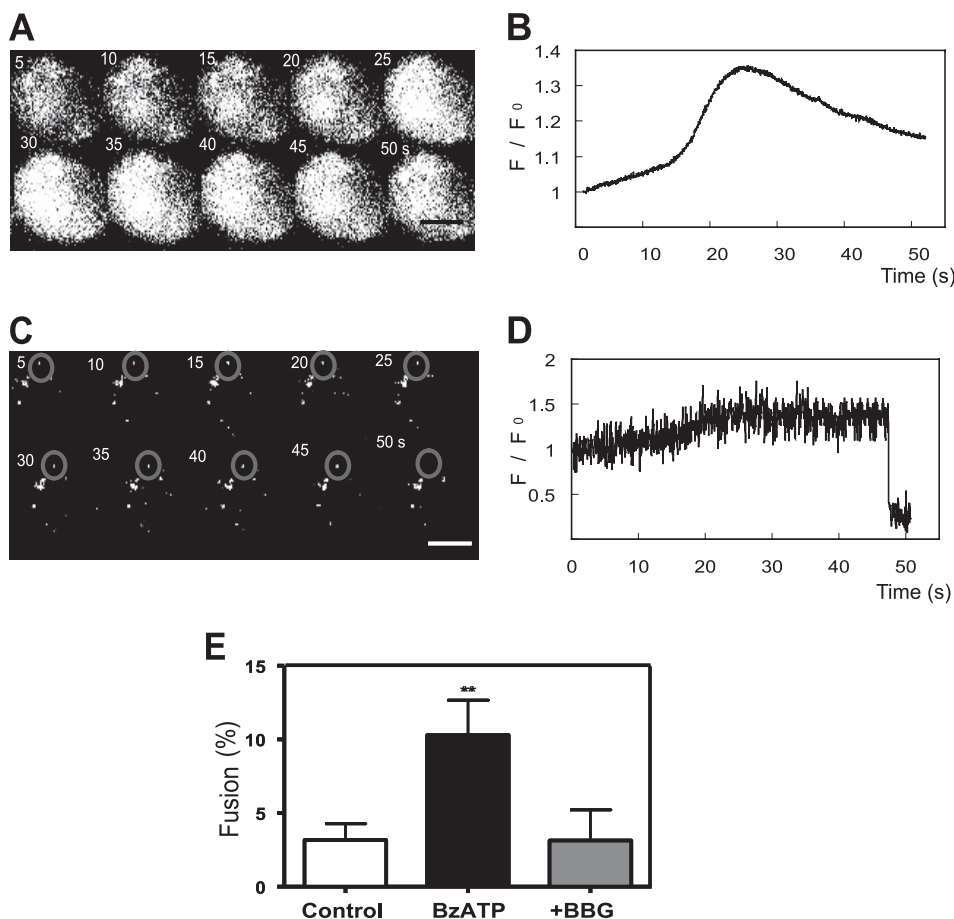


FIGURE 2. P2X7 receptor stimulation increases submembrane $[Ca^{2+}]_i$ and induces LDCV exocytosis from N2a cells. N2a cells were incubated with rhod-2 and quinacrine as described under "Experimental Procedures." Cells were placed in a superfusion chamber, and fluorescence was excited alternating with 488-nm (to excite quinacrine) and 561-nm light (to excite rhod-2) under total internal reflection fluorescence conditions. Images were taken at 50-ms intervals. Bath perfusion with 100 μ M BzATP for 30 s started at $t = 0$. *A*, time-lapse series of images at 5-s intervals of rhod-2 fluorescence from the footprint of a N2a cell after superfusion with BzATP is shown. *B*, shown is the time course of spatially averaged changes in rhod-2 fluorescence from the cell shown in *A*. *C*, shown is a time-lapse series of images at 5-s intervals of quinacrine-labeled vesicles from the footprint of the cell shown in *A*. The gray circle in the upper region of every image denotes a quinacrine-labeled vesicle that is exocytosed between 45 and 50 s after the beginning of BzATP stimulation. *D*, shown is the time-course of quinacrine fluorescence for the region of interest comprised in the circle defined in *C*. The rapid loss of the quinacrine signal at $t \approx 47$ s is apparent. *E*, P2X7 receptor activation increases the frequency of LDCV fusions in N2a cells. Frequency of vesicle fusion was estimated by counting the number of quinacrine-labeled granules lost over 50 s after a change in the superfusion medium and expressed as a percentage of total quinacrine spots. *Control*, Locke's solution ($n = 48$ cells); *BzATP*, BzATP 100 μ M for 30 s ($n = 52$ cells); *+BBG*, BzATP in the presence of BBG 5 μ M ($n = 20$ cells). BBG was administered 5 min before and during BzATP perfusion. Note that the frequency of fusions is significantly ($p < 0.01$) higher in BzATP-stimulated cells as compared with cells superfused with plain Locke's solution or cells stimulated with BzATP in the presence of BBG. Calibration bar in *A* and *C*, 10 μ m.

of the vesicles to the plasma membrane ("docking") and a membrane-delimited maturation process that renders the vesicles fusion-competent ("priming"). As these two processes imply the translocation and the change in mobility of vesicles, it can be directly studied with TIRFM (38). We, thus, performed experiments to characterize the effects of BzATP on LDCV motion in N2a cells as a mean to explore the involvement of P2X7 receptors in the control of processes preceding vesicle exocytosis. To this aim, N2a cells were incubated with LysoTracker red, which labels a small fraction of LDCVs, hence, facilitating the observation of vesicle trajectories devoid of crossings. Given that LysoTracker red fluorescence is excited by 561-nm light, we employed in these experiments fluo-4, a $[Ca^{2+}]_i$ indicator sensitive to 488-nm light. Because LysoTracker red may label acidic organelles other than LDCV, we investigated the degree of coincidence between LysoTracker red fluorescence and that of pGFP-N1-synaptobrevin 2 targeted to the secretory vesicles of N2a cells. As shown in [supplemental](#)

[Fig. S5](#), LysoTracker red produced a clear vesicular pattern under confocal microscopy, whereas pGFP-N1-synaptobrevin 2 gave rise to a more diffused staining, probably indicating the presence of synaptobrevin in several compartments of the granule biogenesis pathway. Quantitative analysis indicated a percentage of coincidence of LysoTracker red pixels with pGFP-N1-synaptobrevin 2 pixels of $75.35 \pm 2.17\%$ with a Pearson's correlation coefficient corresponding to all colocalized pixels of 0.76 ± 0.01 ($n = 9$ cells), thus implying that LysoTracker red extensively labels LDCVs in our cell model.

First, we analyzed the movement of LDCVs in a direction perpendicular to the glass-liquid interface to which the cells adhere (xz plane; axial movement). Inherent to total internal reflection fluorescence is an exponentially decaying excitation light in the xz plane, which causes fluorescently labeled vesicles to appear progressively brighter as they move toward the interface, where the plasma membrane is located. As expected, stimulation of the cells with BzATP (100 μ M for 30 s) produced an

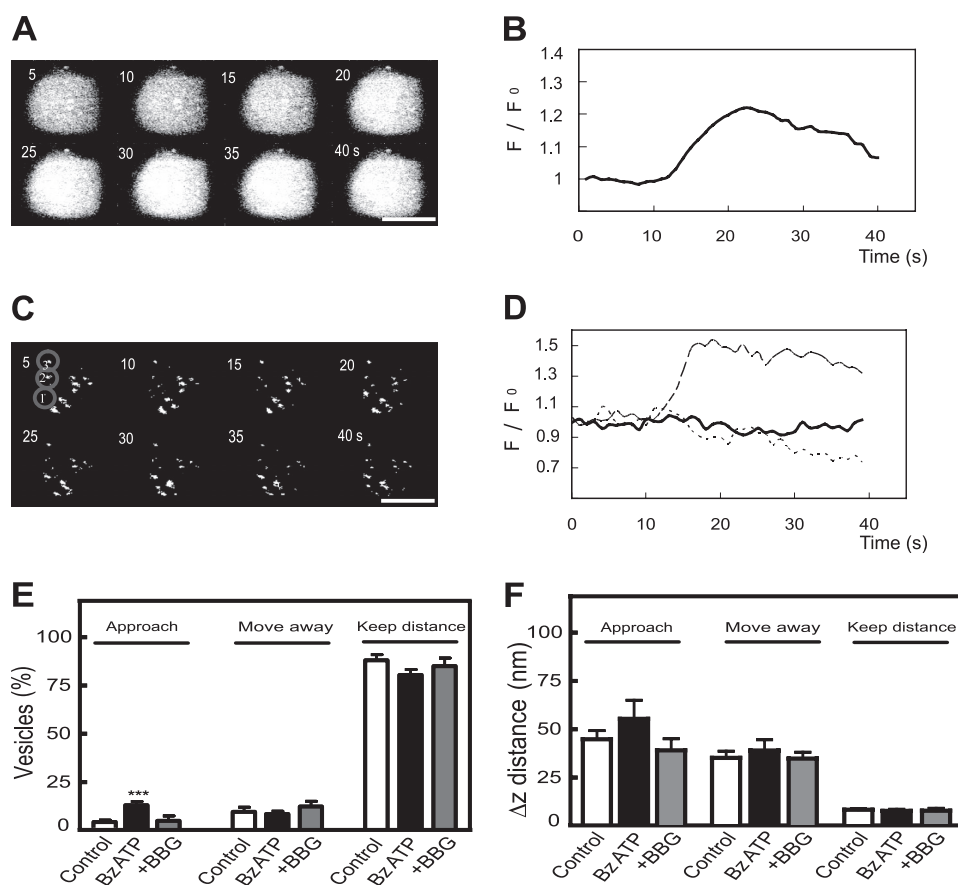


FIGURE 3. P2X7 receptor stimulation modifies axial movement of LDCVs. Cells were loaded with Lysotracker red and fluo-4 as indicated under “Experimental Procedures,” and TIRFM images were taken at 1-s intervals. *A*, shown is a time-lapse series of images at 5-s intervals of fluo-4 fluorescence from the footprint of a N2a cell after superfusion with BzATP ($100\ \mu\text{M}$ for 30 s; initiated at $t = 0$). *B*, shown is the time-course of spatially averaged changes in fluo-4 fluorescence from the cell shown in *A*. *C*, shown is a time-lapse series of images at 5-s intervals of a group of Lysotracker red-tagged vesicles from the footprint of the cell shown in *A*. Changes in vesicle fluorescence over time reflect the movement of the vesicles toward and away from the plasma membrane. Three vesicles representative of different motion behaviors appear encircled and numbered (1, 2, and 3). *D*, shown is the time-course of changes in fluorescence of the regions of interest comprised in the circles drawn in *C*. The dashed line reflects the axial movement of vesicle 1 that approaches the plasma membrane, the dotted line reports on vesicle 2 that moves away from the membrane, and the continuous line refers to vesicle 3 that keeps its distance to the membrane. *E*, P2X7 receptor stimulation increases the fraction of LDCVs approaching the plasma membrane. Relative distribution in non-stimulated N2a cells (Control, 199 vesicles from 42 cells), N2a cells stimulated with $100\ \mu\text{M}$ BzATP (Bz-ATP, 284 vesicles from 57 cells), and N2a cells stimulated with $100\ \mu\text{M}$ BzATP in the presence of $5\ \mu\text{M}$ BBG (+BBG, 95 vesicles from 18 cells) of three groups of LDCVs defined according to their type of movement in the xz plane; left bars, vesicles approaching the membrane; middle bars, vesicles moving away from the plasma membrane; right bars, vesicles keeping their distance to the membrane. BBG was administered 5 min before and during BzATP perfusion. Note that the population of vesicles that gets closer to the membrane in BzATP-stimulated cells is significantly ($p < 0.005$) larger than in control cells or BzATP-stimulated cells in the presence of BBG. *F*, Δz distance covered by vesicles within the three different axial movement groups from non-stimulated N2a cells (Control), N2a cells stimulated with $100\ \mu\text{M}$ BzATP (Bz-ATP), and N2a cells stimulated with $100\ \mu\text{M}$ BzATP in the presence of $5\ \mu\text{M}$ BBG (+BBG) is shown. LDCVs analyzed were the same as in *E*. Calibration bar in *A* and *C*, $10\ \mu\text{m}$.

increase in fluo-4 fluorescence, reflecting the rise in $[\text{Ca}^{2+}]_i$ (Fig. 3, *A* and *B*; supplemental Video S4). This was accompanied by changes in the fluorescence intensity of Lysotracker red-tagged vesicles (Fig. 3, *C* and *D*; supplemental Video S5) such that a number of vesicles became brighter (see vesicle 1 in Fig. 3*C* and the dashed line in Fig. 3*D*), whereas others underwent small fluorescence decreases (vesicle 2 in Fig. 3*C* and the dotted line in Fig. 3*D*), and still others did not show any significant change in fluorescence (vesicle 3 in Fig. 3*C* and the continuous line in Fig. 3*D*). Such a differential behavior in vesicle fluorescence led us to classify LDCVs into three groups according to their axial movement; 1) vesicles approaching the plasma membrane, 2) vesicles moving away from it, and 3), vesicles keeping their position with respect to the membrane. We have evaluated the relative distribution of the three vesicle populations in non-stimulated cells, BzATP-stimulated cells, and BzATP-stimulated cells in the presence of BBG (Fig. 3*E*). Because the

loading with Lysotracker red showed variability between cells and between LDCVs of the same cell and also because of the possible existence of infoldings in the plasma membrane, we did not infer the absolute z position of the vesicles from its fluorescence intensity but only estimated the Δz change. We set a vertical displacement of $\pm 15\ \text{nm}$ from the initial position as the minimum that a vesicle should move for being assigned to one of the two first groups (namely, vesicles approaching or leaving the membrane). BzATP stimulation increased by 4-fold the percentage of vesicles approaching the membrane ($11.91 \pm 1.9\%$; $n = 57$ cells) in comparison with non-stimulated cells ($3.0 \pm 1.0\%$; $n = 42$ cells) or cells stimulated with BzATP in the presence of BBG ($3.5 \pm 1.9\%$; $n = 18$ cells). The population of vesicles moving away from the membrane was also a minor one (7–12%), although its importance did not vary significantly among the three conditions considered. Last, vesicles keeping their position relative to the plasma membrane constituted the

P2X7 Receptor-mediated ATP Exocytosis in Neuroblastoma Cells

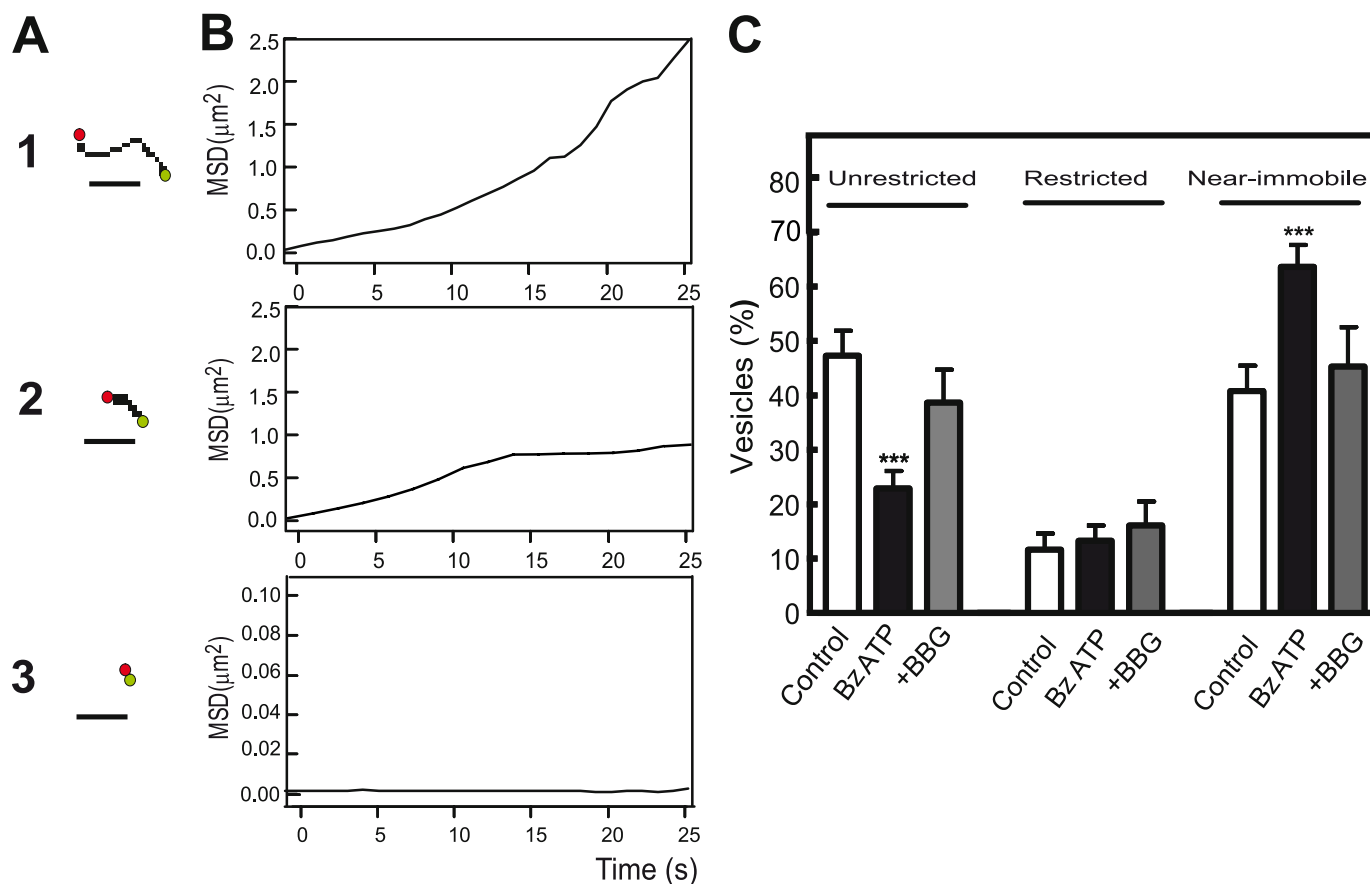


FIGURE 4. P2X7 receptor stimulation reduces parallel movement of LDCVs. *A*, vesicle trajectories in the *xy* plane are shown. Three types of movement were distinguished on the basis of maximal displacement of the vesicles within a time window of 25 s: unrestricted movement (exemplified by the vesicle in *A1*), restricted movement (exemplified by the vesicle shown in *A2*), and near immobility (exemplified by the vesicle shown in *A3*). *Green dots* show the initial position in the trajectory, and *red dots* show the end position. Calibration bar, 1 μm . *B*, shown are mean square displacements (*MSD*) at different time intervals from the trajectories shown in *A*. *C*, relative distribution in non-stimulated N2a cells (*Control*, 199 vesicles from 42 cells), N2a cells stimulated with 100 μM BzATP (*Bz-ATP*, 284 vesicles from 57 cells), and N2a cells stimulated with 100 μM BzATP in the presence of 5 μM BBG (*+BBG*, 95 vesicles from 18 cells) of LDCV pools defined according to their type of movement in the *xy* plane; *left bars*, unrestricted motion; *middle bars*, restricted motion; *right bars*, near immobility. Note that the fraction of near immobile vesicles in BzATP-stimulated cells is significantly larger than in control cells, and the fraction of vesicles with unrestricted motion has been comparatively reduced ($p < 0.005$ in both cases).

largest population, contributing 80–90% of the vesicles tagged with Lysotracker red irrespective of the experimental conditions. Interestingly, the average displacement (Δz distance) of the vesicles within each particular group was quite constant across the three experimental situations (Fig. 3*F*).

Next, we studied vesicle motion in the plane parallel to the glass-liquid interface (*xy* plane; parallel movement). After representing vesicle trajectories obtained by tracking LDCV centroids, we could distinguish three movement patterns based on the maximal displacement of the vesicles: 1) unrestricted mobility, 2) restricted caged mobility, and 3) near immobility (Fig. 4*A*, 1–3). Because picking a specific distance for the analysis proved difficult due to large differences in net translocation among individual granules, we decided to differentiate between types of vesicle mobility by analyzing the plot of the mean square displacement against incrementing time intervals (23, 39–42). This method allows the distinction between immobile and mobile vesicles from the slope of the plot at $x \rightarrow 0$; likewise, a negative curvature of the plot indicates a restricted motion, whereas a linear increase or a positive curvature of mean square displacement *versus* time would indicate a free random or

directed motion (namely, the unrestricted type of motion) (Fig. 4*B*, 1–3).

Under control conditions (perfusion with a Locke's solution), the fraction of vesicles displaying an unrestricted random or directed type of movement was $47.59 \pm 4.57\%$ ($n = 42$ cells), whereas those displaying a restricted motion accounted for $11.62 \pm 2.99\%$ of the vesicles; likewise, near immobile vesicles were $40.81 \pm 4.68\%$ of all vesicles analyzed. Upon stimulation with 100 μM BzATP (30 s), there was a statistically significant increment in the fraction of immobile vesicles ($63.63 \pm 3.97\%$; $n = 57$ cells), this increment being associated with a reduction in the fraction of those displaying an unrestricted type of movement ($22.91 \pm 3.19\%$). Importantly, pretreatment with 5 μM BBG prevented the effect of BzATP on vesicle movement in the *xy* plane, thus confirming the involvement of P2X7 receptors (Fig. 4*C*). Collectively, these findings indicate that in addition to trigger exocytosis, P2X7 receptor activation profoundly modifies secretory vesicle dynamics in N2a cells.

N2a Cells Express Major Synaptic Proteins and the Vesicular Monoamine and Nucleotide Transporters—The above-reported functional studies demonstrate that P2X7 receptor acti-

vation triggers exocytosis from N2a cells. However, both the proteins mediating vesicle fusion and the type of cargo stored and released are not known. Because neuroblastoma cells arise from neural crest precursors of the sympathetic nervous system, we set out to investigate whether N2a cells express prominent members of the secretory machinery involved in calcium-dependent neuroexocytosis. Hence, the expression of the three members, SNAP-25, syntaxin 1, and synaptobrevin/VAMP, of the neuronal SNARE membrane fusion complex and other proteins involved in synaptic exocytosis was analyzed by immunocytochemistry or RT-PCR (supplemental Fig. S6). In N2a cells, SNAP-25 and syntaxin 1A were predominantly localized at the plasma membrane as already reported (26). At variance, vesicle-resident proteins such as synaptophysin and synaptobrevin showed a broad intracellular distribution. Moreover, synapsin 1, a protein involved in regulating the number of synaptic vesicles available for exocytotic release (43), also showed a cytosolic location in N2a cells. Likewise, the expression of vesicular monoamine transporters 1 and 2 (VMAT-1 and VMAT-2) as markers of catecholamine-storing vesicles was investigated. Both transporter proteins were detected in N2a cells and localized in the cytosolic compartment (supplemental Fig. S6A). Interestingly, a high level of the vesicular nucleotide transporter transcript was also observed in N2A cells (supplemental Fig. S6B), suggesting that ATP and other nucleotidic compounds could be co-stored with catecholamines and released by exocytosis in a Ca^{2+} -dependent manner.

N2a Cells Release ATP—To confirm the ability of N2a cells to release ATP, we set out to use the very sensitive luciferin-luciferase assay to quantify ATP in the extracellular medium under experimental conditions that either facilitated or inhibited Ca^{2+} -dependent exocytosis (Fig. 5). Basal ATP release was fairly low (≈ 15 pM) irrespective of the presence or the absence of the ecto-ATPase inhibitor ARL 67156 ($100 \mu\text{M}$) in the culture medium. The Ca^{2+} -selective ionophore, ionomycin ($10 \mu\text{M}$), increased the ATP concentration to 75 pM, this value being more than doubled in the presence of ARL 67156. This result indicates that ATP release depends on an elevation of $[\text{Ca}^{2+}]_i$ and, hence, suggests it can involve an exocytotic mechanism. The participation of SNARE proteins in such a release process was confirmed by using (i) NEM ($500 \mu\text{M}$), which strongly inhibited both basal and ionomycin-induced ATP release (Fig. 5, A and B), and (ii) BoNT/A (30 nM; 72 h), which reduced by $62.25 \pm 5.11\%$ ($n = 3$ experiments performed in triplicate) the net release of ATP induced by ionomycin (supplemental Fig. S4).

P2X7 Receptors Trigger Quantal ATP Release—If the release of ATP from N2a cells were exocytotic, then it would be possible to detect it as STICs, reminiscent of ATP-mediated postsynaptic currents, provided that the sensor cell and the ATP-releasing one were sufficiently close to each other (44). We, therefore, decided to allow the growth of N2a cells in coverslips for 48 h so that they almost reached confluency and to patch clamp only those cells included in clusters comprising 5–20 individual cells (supplemental Fig. S7A). In resting conditions, the occurrence of STICs was very infrequent (0.02 ± 0.01 Hz; calculated for a 120 s observation time in 6 cells), likely indicating a low rate of spontaneous ATP release (Fig. 6, A and E). The

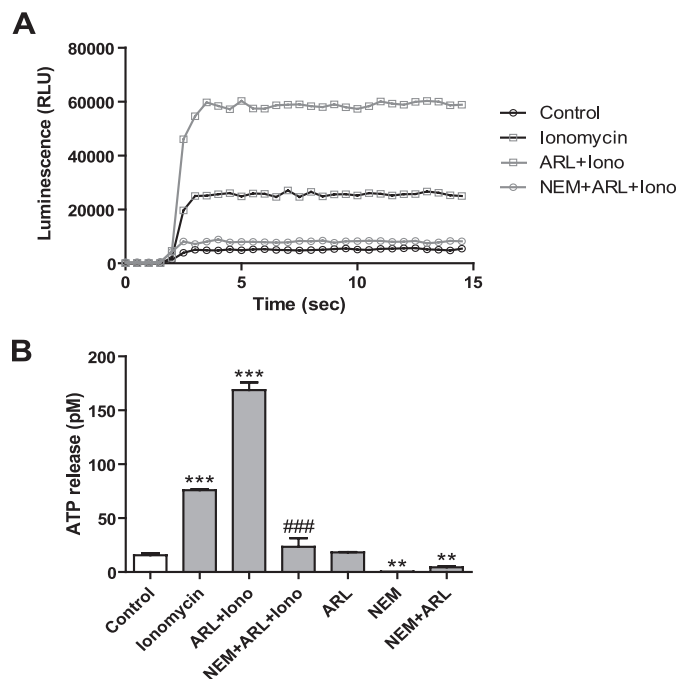


FIGURE 5. N2a cells release ATP by a NEM-sensitive mechanism. A, shown are representative records of luminescence evoked by ATP released into the extracellular medium of N2a cells before (Control) and after ionomycin ($10 \mu\text{M}$) stimulation in the absence (ionomycin) or presence of the ecto-ATPase inhibitor ARL67156 ($100 \mu\text{M}$; ARL + Iono) or ARL67156 plus the exocytosis inhibitor NEM ($500 \mu\text{M}$; NEM + ARL + Iono). Extracellular medium was collected after a 5-min exposure of the cells to each of the different experimental conditions. Luminescence is expressed as relative light units (RLU). B, quantification of ATP release under the different experimental conditions is shown. Each bar represents the mean \pm S.E. of the results from three experiments. A calibration curve generated with serial dilutions of an ATP standard was used to convert luminescence units into ATP concentration values. **, $p < 0.005$; ***, $p < 0.001$ with respect to control; ###, $p < 0.001$ compared with ARL67156 + ionomycin.

mean amplitude of STICs in resting conditions was 10.36 ± 0.23 pA, with a rise time (20–80%) of 4.6 ± 0.56 ms and a half-decay time of 6.72 ± 0.48 ms (11 spikes from 6 cells). Similarly to TIRFM and capacitance measurement experiments, we looked for the effect on the incidence of STICs of BzATP ($100 \mu\text{M}$ for 10 s) applied by pressure from a patch pipette located some μm away from the recorded cell. BzATP generated a slowly rising current that returned to base line once drug administration was stopped (Fig. 6A). Both during BzATP application and the washout phase, there was an increase in the appearance of STICs (0.086 ± 0.02 Hz; 62 STICs from 6 cells), which nevertheless exhibited similar amplitude and kinetics as that of STICs recorded in resting conditions (Fig. 6D). The fast time course of STICs suggested that they could arise from vesicular ATP released by BzATP stimulation. To get insight into the mechanism of STIC generation, we first investigated the dependence on extracellular Ca^{2+} of STIC occurrence. To this aim, cells were bathed in a Ca^{2+} -free solution containing 1 mM Mg^{2+} so that currents elicited by BzATP in the presence or absence of external Ca^{2+} displayed similar amplitudes (data not shown). Under these conditions much fewer STICs were detected after BzATP stimulation (17 STICs from 5 cells; 0.029 ± 0.08 Hz), suggesting that BzATP-induced STICs were dependent on influx of extracellular Ca^{2+} (Fig. 6, B and E). We also tested the effect of ionomycin ($5 \mu\text{M}$) on the incidence of

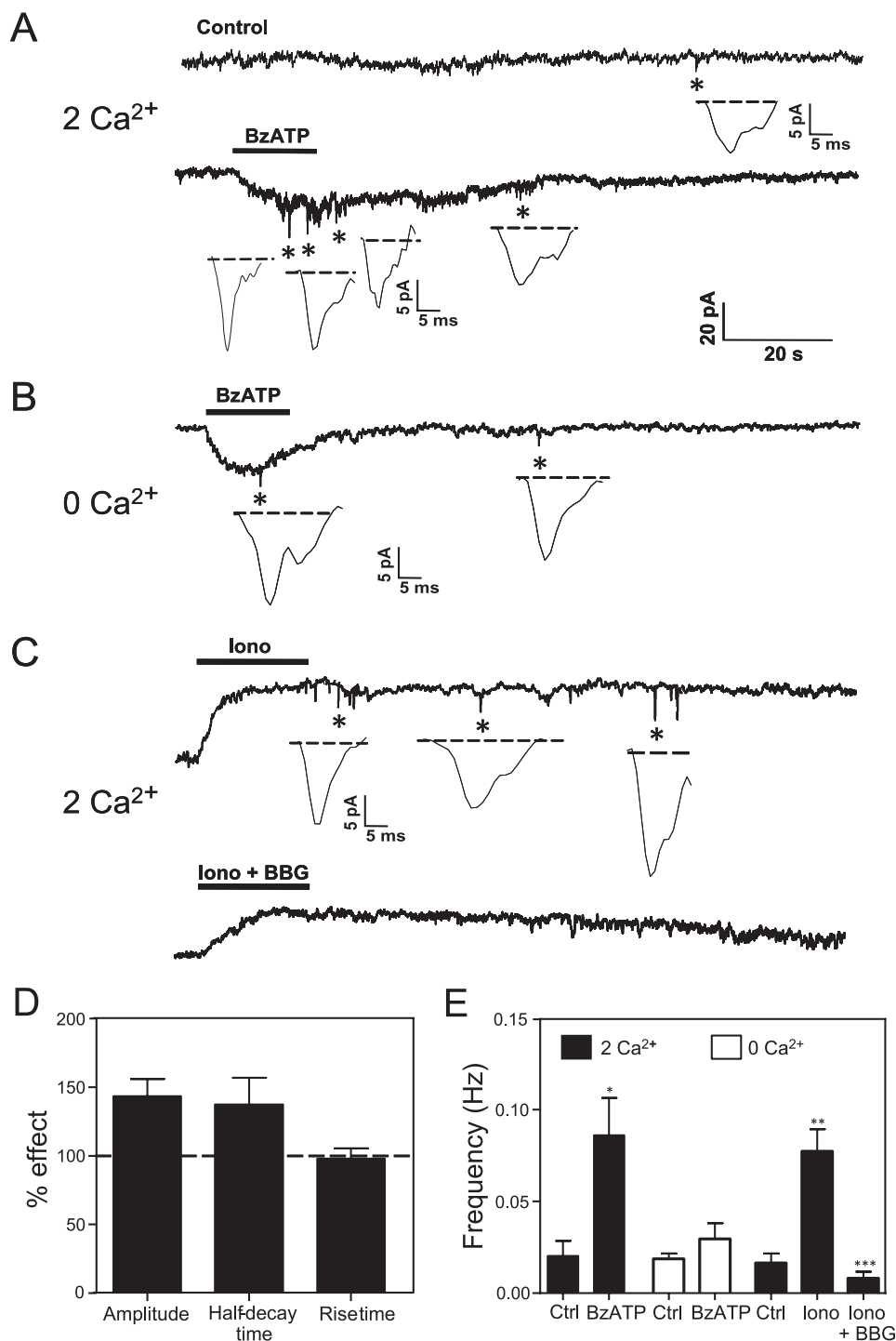


FIGURE 6. **Detection of small transient inward currents (STICs) in N2a cells.** *A, upper panel*, spontaneous STIC (*) recorded in a N2 cell bathed in a standard (2.5 mM Ca²⁺)-containing extracellular solution (*Control*) is shown. *Lower panel*, shown is a local application of BzATP (100 μM for 10 s) from a patch pipette to the same cell that generated STICs (*) during the BzATP-induced inward current and during washout. *B*, shown are STICs (*) generated by BzATP in a N2a cell bathed in a 0 Ca²⁺-containing extracellular solution. *C*, STICs (*) generated by local application of ionomycin (10 μM for 15 s; *Iono*) in two different N2a cells bathed in an standard extracellular saline in the absence (*upper panel*) or presence of BBG (5 μM) (*lower panel*). Below each asterisk the corresponding STIC is shown at an expanded current and time scale. $V_h = -70$ mV. *D*, STICs generated by BzATP application did not differ from those recorded under control conditions. The values for the amplitude, rise time (20–80%), and half-decay time were normalized to the mean parameter values of STICs detected in control conditions. Nine STICs in control conditions and 62 STICs after application of BzATP were included in the analysis ($n = 6$ cells). *E*, mean frequency of STICs recorded under different experimental conditions is shown. The first four bars to the left represent the mean frequency of STICs recorded in the standard (2 Ca²⁺; $n = 6$ cells) or a Ca²⁺-free (0 Ca²⁺; $n = 5$ cells) extracellular solution before (*Ctrl*) and after BzATP (*BzATP*) application; the first three bars from the right represent the mean frequency of STICs recorded in standard (2 Ca²⁺) extracellular solution before (*Ctrl*) and after ionomycin application in the absence (*Iono*; $n = 6$ cells) and presence of BBG (*Iono + BBG*; $n = 5$ cells). *, $p < 0.05$; **, $p < 0.001$; ***, $p < 0.005$ with respect to its corresponding control.

STICs. As Fig. 6, C and E show, besides eliciting a long-lasting outward current possibly reflecting the activation of a Ca^{2+} -dependent K^+ conductance (45), ionomycin increased the frequency of STICs (0.077 ± 0.012 Hz; 55 STICs from 6 cells), thus implying a relation with an elevation of $[\text{Ca}^{2+}]_i$. Confirmation that STICs were indeed mediated by P2X7 receptors was obtained by adding BBG to the bath solution. Consistent with our expectations, treatment with BBG (5 μM ; added to the bath and puffer pipette solutions) abolished STICs evoked by ionomycin (0.0085 ± 0.0002 Hz; 5 cells) (Fig. 6, C and E). It is also worth mentioning that no significant differences in size and kinetics were observed among STICs detected under the different experimental conditions (supplemental Fig. S6, B–D). Moreover, no correlation was found between the amplitude and decay time of the STICs detected in all experiments ($r = 0.61$). Altogether, these results indicate that endogenous ATP acting on P2X7 receptors generates STICs and that P2X7 receptor stimulation can elicit vesicular ATP release.

DISCUSSION

ATP and its metabolites have now achieved a full and possibly unique status as ubiquitous extracellular messengers. In the nervous system, adenine nucleotides have been involved in intercellular communication between neurons and between neurons and glial cells as well as in the control of cell proliferation, migration, and differentiation (46). The latter roles are essential in supporting brain development, maturation, and repair after either acute injuries or chronic degenerative processes (47). Given the ubiquitous distribution of ATP, an adequate performance of such a variety of functions requires the existence of not only a rich repertoire of purinergic receptors with differential affinity and coupling to intracellular signaling pathways but also a tight control of the availability of the signaling molecule in the extracellular space. On the other hand, cell heterogeneity of primary neuronal cultures and the need to reduce animal use in biomedical research have made clonal cell lines from neuroectodermal origin a convenient experimental model to study basic mechanisms in neural cell signaling. Recently, we have reported that P2X7 receptor inhibition promotes neurogenesis from N2a murine neuroblastoma cells and axonal growth in rat hippocampal neurons (12, 13). By allowing the entrance of small cations into the cell, P2X receptors may also be coupled to some rapid signaling pathways, like those responsible for the control of membrane excitability and the exocytotic release of neurotransmitters. Interestingly, P2X7 receptors are the only members of the ionotropic family of purinergic receptors functionally expressed in N2a cells (12, 48), a cell type that does not show voltage-gated Ca^{2+} entry when kept in a non-differentiated state.⁵ These two facts make this cell system an ideally suited model to study the direct coupling of P2X7 receptors to exocytosis. In the present study, by employing high resolution techniques (patch clamp and TIRFM imaging), we have been able to demonstrate that P2X7 receptor activation not only triggers exocytosis but also pro-

foundly modifies secretory vesicle dynamics in N2a cells. Moreover, immunocytochemical and molecular biological data indicate that these cells express essential proteins involved in exocytosis and have the capability of storing catecholamines and nucleotides in secretory vesicles. Likewise, biochemical measurements demonstrate that N2a cells secrete ATP by an SNARE-dependent exocytotic mechanism. Last, P2X7 receptors have also been shown to mediate the generation of STICs reflecting quantal ATP release, whose incidence is increased by agents that elevate $[\text{Ca}^{2+}]_i$ (ionomycin and the P2X7 receptor agonist, BzATP) and diminished in the absence of extracellular Ca^{2+} .

Membrane capacitance measurements are commonly used as a single-cell assay of exocytosis. Our results indicate that short (few seconds) pulses of BzATP trigger capacitance increases in the 10s of femtofarads range. Taken the value of 1.9 femtofarads for the capacitance of a single chromaffin granule (49), the catecholamine and ATP-storing LDCV from adrenomedullary chromaffin cells, we estimate that on average our stimulation paradigm induces the exocytosis of ≈ 40 LDCVs from N2a cells. Interestingly, such a response, which involves vesicular fusion due to its sensitivity to NEM, can be attributed to the activation of P2X7 receptors as it is not observed under basal (saline superfusion) conditions and, for its major part, is prevented when BzATP-activated currents are inhibited by BBG, a P2X7 receptor antagonist. In comparison with previous work on human neuroblastoma cells reporting small increases (3–4 times the basal values) in substance P release after 2 h of stimulation with nucleotides (15), the results presented here, besides demonstrating a direct coupling (our recording conditions effectively isolate P2X7 receptor-mediated currents) between P2X7 receptors and exocytosis in N2a cells, illustrate the ability of this cell line to rapidly and efficiently undergo exocytosis.

Electrophysiological data were complemented by TIRFM imaging, which allows the observation of individual secretory vesicles in real time during exocytosis. After loading N2a cells with quinacrine, we were able to detect diffraction-limited (≈ 400 -nm diameter) fluorescent spots representing ATP-containing vesicles (32, 34, 50) located in the submembrane region of the cell. Moreover, by simultaneously loading the cells with rhod-2, a $[\text{Ca}^{2+}]_i$ indicator dye, we could also monitor changes in $[\text{Ca}^{2+}]_i$ in the cell region where exocytosis occurs. Exocytosis was detected by the rapid loss of quinacrine fluorescence, and release efficacy was estimated as the fraction of labeled-vesicles exocytosed in a given time period (50 s). Under control conditions, there were not significant changes in rhod-2 fluorescence, whereas the fraction of vesicles exocytosed was of 3%. Importantly, upon BzATP application, both a rise in submembrane $[\text{Ca}^{2+}]_i$ and a 3-fold increase in the number of exocytotic events were observed. It should be noted that the idea that the cell region in contact with the culture support (the footprint) can show exocytosis is consistent with a wealth of information derived from TIRFM imaging employing vesicular membrane markers (51) and with electron microscopy studies (52) and is also in line with our results on the BoNT/A and NEM sensitivity of the quinacrine-fluorescence loss events. Both submembrane $[\text{Ca}^{2+}]_i$ increases and the accompanying vesicular exocytosis

⁵ Y. Gutiérrez-Martín, D. Bustillo, R. Gómez-Villafuertes, J. Sánchez-Nogueiro, C. Torregrosa-Hetland, T. Binz, L. M. Gutiérrez, M. T. Miras-Portugal, and A. R. Artalejo, unpublished data.

can be directly attributed to P2X7 receptor activation, as they were reduced to near control values in the presence of BBG. The observation that only about 10% of the LDCVs that are exposed to a submembrane $[Ca^{2+}]_i$ elevation is released indicates that proximity to the plasma membrane does not ensure release readiness and that vesicles have to undergo docking and a priming process to achieve full release competence (53–55). Both processes can be directly studied by TIRFM, as they have been related to changes in vesicle mobility (53). Therefore, docking has been shown to correspond to changes in the axial mobility (56, 57), whereas priming is associated with restricted lateral motion (40). Similarly to what has been reported for embryonic mouse chromaffin cells (56), most of the LDCVs seen at the footprint of N2a cells are stably docked at the plasma membrane. Axial movement leading to either vesicle docking (movement toward the membrane) or undocking (movement away from the membrane) was observed for a relatively small fraction of the vesicles. Noteworthy, P2X7 receptor stimulation was associated with a significant increase in the fraction of vesicles that approached the plasma membrane. This can be interpreted as if P2X7 receptors could control the rate of vesicle delivery from the cell interior, this effect being crucial to support secretion over sustained stimulation. Interestingly, vesicle supply and docking at the plasma membrane are two processes interlinked by the action of Munc 18-1, a cytosolic protein known to enhance morphological vesicle docking by interacting both with the plasma membrane SNARE, syntaxin, and the actin cytoskeleton (58–60). In neurons and neuroendocrine cells, docked vesicles need to undergo priming before they can be released. Primed vesicles constitute the readily releasable pool of vesicles and can be rapidly exocytosed in response to an elevation in $[Ca^{2+}]_i$. Priming requires the formation of the ternary SNARE complex between syntaxin, SNAP-25, and synaptobrevin/VAMP (53) and has been associated with vesicle immobilization (40, 61). In resting N2a cells, about 45% of the vesicles visualized at the footprint appear as near immobile in the plane parallel to the membrane. P2X7 receptor stimulation leads to an increase in the fraction of immobile vesicles and a concomitant reduction of those exhibiting unrestricted mobility. These two effects imply an overall decrease in lateral mobility of the vesicles located within the evanescent field and, therefore, are consistent with enhanced vesicle priming. Our results also point to a concomitant increase in the fraction of immobile vesicles and in the rate of exocytosis. Both effects are mutually compatible by considering the different dependence on $[Ca^{2+}]_i$ of vesicle priming and exocytosis (62) and that the former is accelerated at physiological temperature (63). Hence, under our experimental condition of 37 °C and with the moderate $[Ca^{2+}]_i$ elevation elicited by BzATP, it is feasible to induce an overfilling of the readily releasable pool, whereas the cell exhibits a modest secretory response (64). Altogether, the functional results so far discussed indicate that P2X7 receptor stimulation affects multiple steps (vesicle delivery, docking, priming, and exocytosis) in the regulated-secretion pathway of N2a cells. Most likely, this is a consequence of the ability of $[Ca^{2+}]_i$, which is elevated after P2X7 receptor activation, to control secretion in a way that ensures both a fast secretory response due to the release of the readily releasable pool of vesicles and a sustained

secretion by promoting the delivery of vesicles to the exocytotic sites at the plasma membrane as well and their priming to achieve release competence (65–67).

Our results add to the existing evidence implicating P2X receptors in neurotransmitter and hormone release from neurons and neuroendocrine cells (68). N2a cells express the three neuronal SNAREs, which are involved in the docking, priming, and fusion steps of regulated exocytosis (69–71). Moreover, in accordance with their origin from precursors of sympathetic neurons, they are endowed with LDCVs specialized in the storage of catecholamines and ATP. Our experiments also support the notion that ATP transported into secretory granules (72) can be released by exocytosis after a rise in $[Ca^{2+}]_i$ brought about by ionomycin and by P2X7 receptor activation. We have reached this conclusion by a biochemical determination of ATP release but also by using N2a cells as biosensors to detect their own ATP release. Hence, in response to stimulation by either ionomycin or BzATP, we recorded STICs that were mediated by ATP acting on P2X7 receptors due to their sensitivity to BBG. In addition, the fast kinetics of STICs and the non-desensitizing characteristics of P2X receptor-mediated responses suggest that STICs are based on non-equilibrium ATP gradients like those expected to arise from a vesicular type of release. Furthermore, the extracellular Ca^{2+} dependence of STIC occurrence is fully in accordance with the involvement of a classical exocytotic mechanism. Taking into account our previous results indicating that P2X7 receptors activated by endogenously released ATP exert a tonic inhibition of neuron-like differentiation of N2a cells (12, 13), the present results implicating P2X7 receptors in exocytosis prompt us to propose the existence of an autocrine/paracrine positive feedback mechanism by which P2X7 receptors would mediate the exocytotic release of ATP that, in turn, would act on P2X7 receptors on the same or neighbor cells to further stimulate its own release and negatively control cell differentiation. Likewise, our results point out the suitability of N2a cells as a model system to characterize the physiology of vesicular release of ATP and to explore many of the complex intra- and intercellular signaling networks controlled by ATP in both the central and peripheral nervous system.

REFERENCES

1. Burnstock, G., and Kennedy, C. (1985) *Gen. Pharmacol.* **16**, 433–440
2. von Kügelgen, I., and Wetter, A. (2000) *Naunyn-Schmiedeberg's Arch. Pharmacol.* **362**, 310–323
3. Khakh, B. S., Burnstock, G., Kennedy, C., King, B. F., North, R. A., Séguéla, P., Voigt, M., and Humphrey, P. P. (2001) *Pharmacol. Rev.* **53**, 107–118
4. North, R. A. (2002) *Physiol. Rev.* **82**, 1013–1067
5. Jarvis, M. F., and Khakh, B. S. (2009) *Neuropharmacology* **56**, 208–215
6. Huang, N., Wang, D. J., and Heppel, L. A. (1989) *Proc. Natl. Acad. Sci. U.S.A.* **86**, 7904–7908
7. Brändle, U., Zenner, H. P., and Ruppersberg, J. P. (1999) *Neurosci. Lett.* **273**, 105–108
8. Adrian, K., Bernhard, M. K., Breiting, H. G., and Ogilvie, A. (2000) *Biochim. Biophys. Acta* **1492**, 127–138
9. Heo, J. S., and Han, H. J. (2006) *Stem Cells* **24**, 2637–2648
10. Deli, T., and Csernoch, L. (2008) *Pathol. Oncol. Res.* **14**, 219–231
11. White, N., and Burnstock, G. (2006) *Trends J. Pharmacol. Sci.* **27**, 211–217
12. Gómez-Villafuertes, R., del Puerto, A., Díaz-Hernández, M., Bustillo, D., Díaz-Hernández, J. I., Huerta, P. G., Artalejo, A. R., Garrido, J. J., and Miras-Portugal, M. T. (2009) *FEBS J.* **276**, 5307–5325

13. Díaz-Hernandez, M., del Puerto, A., Díaz-Hernandez, J. I., Diez-Zaera, M., Lucas, J. J., Garrido, J. J., and Miras-Portugal, M. T. (2008) *J. Cell Sci.* **121**, 3717–3728
14. Muñoz, M., Rosso, M., Pérez, A., Coveñas, R., Rosso, R., Zamarrigo, C., and Piruat, J. I. (2005) *Neuropeptides* **39**, 427–432
15. Raffaghello, L., Chiozzi, P., Falzoni, S., Di Virgilio, F., and Pistoia, V. (2006) *Cancer Res.* **66**, 907–914
16. Pellegatti, P., Falzoni, S., Pinton, P., Rizzuto, R., and Di Virgilio, F. (2005) *Mol. Biol. Cell* **16**, 3659–3665
17. Rummel, A., Mahrhold, S., Bigalke, H., and Binz, T. (2004) *Mol. Microbiol.* **51**, 631–643
18. Hamill, O. P., Marty, A., Neher, E., Sakmann, B., and Sigworth, F. J. (1981) *Pflugers Arch.* **391**, 85–100
19. Lindau, M., and Neher, E. (1988) *Pflugers Arch.* **411**, 137–146
20. Carabelli, V., Giancippoli, A., Baldelli, P., Carbone, E., and Artalejo, A. R. (2003) *Biophys. J.* **85**, 1326–1337
21. Wu, Z. X., Xia, S., Xu, L., Bai, L., and Xu, T. (2003) *Sheng wu hua xue yu sheng wu wu li xue bao Acta biochimica et biophysica Sinica* **35**, 381–386
22. Qian, H., Sheetz, M. P., and Elson, E. L. (1991) *Biophys. J.* **60**, 910–921
23. Johns, L. M., Levitan, E. S., Shelden, E. A., Holz, R. W., and Axelrod, D. (2001) *J. Cell Biol.* **153**, 177–190
24. Lévesque, S. A., Lavoie, E. G., Lecka, J., Bigonnesse, F., and Sévigny, J. (2007) *Br. J. Pharmacol.* **152**, 141–150
25. Chevrier, D., Fournier, H., Nault, C., Zollinger, M., Crine, P., and Boileau, G. (1991) *Mol. Cell. Endocrinol.* **79**, 109–118
26. Koticha, D. K., McCarthy, E. E., and Baldini, G. (2002) *J. Cell Sci.* **115**, 3341–3351
27. Neher, E., and Marty, A. (1982) *Proc. Natl. Acad. Sci. U.S.A.* **79**, 6712–6716
28. Jiang, L. H., Mackenzie, A. B., North, R. A., and Surprenant, A. (2000) *Mol. Pharmacol.* **58**, 82–88
29. Söllner, T., Whiteheart, S. W., Brunner, M., Erdjument-Bromage, H., Geromanos, S., Tempst, P., and Rothman, J. E. (1993) *Nature* **362**, 318–324
30. Xu, T., Ashery, U., Burgoyne, R. D., and Neher, E. (1999) *EMBO J.* **18**, 3293–3304
31. Luna, C., Li, G., Qiu, J., Challa, P., Epstein, D. L., and Gonzalez, P. (2009) *Invest. Ophthalmol. Vis. Sci.* **50**, 5805–5810
32. Bodin, P., and Burnstock, G. (2001) *J. Cardiovasc. Pharmacol.* **38**, 900–908
33. Coco, S., Calegari, F., Pravettoni, E., Pozzi, D., Taverna, E., Rosa, P., Matteoli, M., and Verderio, C. (2003) *J. Biol. Chem.* **278**, 1354–1362
34. Pangrsic, T., Potokar, M., Stenovc, M., Kreft, M., Fabbretti, E., Nistri, A., Pryazhnikov, E., Khiroog, L., Giniatullin, R., and Zorec, R. (2007) *J. Biol. Chem.* **282**, 28749–28758
35. Becherer, U., Moser, T., Stühmer, W., and Oheim, M. (2003) *Nat. Neurosci.* **6**, 846–853
36. Lev-Ram, V., Miyakawa, H., Lasser-Ross, N., and Ross, W. N. (1992) *J. Neurophysiol.* **68**, 1167–1177
37. Blasi, J., Chapman, E. R., Link, E., Binz, T., Yamasaki, S., De Camilli, P., Südhof, T. C., Niemann, H., and Jahn, R. (1993) *Nature* **365**, 160–163
38. Becherer, U., Pasche, M., Nofal, S., Hof, D., Matti, U., and Rettig, J. (2007) *PLoS ONE* **2**, e505
39. Giner, D., López, I., Villanueva, J., Torres, V., Viniegra, S., and Gutiérrez, L. M. (2007) *Neuroscience* **146**, 659–669
40. Nofal, S., Becherer, U., Hof, D., Matti, U., and Rettig, J. (2007) *J. Neurosci.* **27**, 1386–1395
41. Oheim, M., and Stühmer, W. (2000) *Eur. Biophys. J.* **29**, 67–89
42. Steyer, J. A., and Almers, W. (1999) *Biophys. J.* **76**, 2262–2271
43. Yamamoto, H., Matsumoto, K., Araki, E., and Miyamoto, E. (2003) *J. Pharmacol. Sci.* **93**, 30–34
44. Fabbro, A., Skorinkin, A., Grandolfo, M., Nistri, A., and Giniatullin, R. (2004) *J. Physiol.* **560**, 505–517
45. Leinders, T., and Vijverberg, H. P. (1992) *Pflugers Arch.* **422**, 223–232
46. Burnstock, G. (2006) *Pharmacol. Rev.* **58**, 58–86
47. Burnstock, G. (2008) *Nat. Rev. Drug Discov.* **7**, 575–590
48. Wu, P. Y., Lin, Y. C., Chang, C. L., Lu, H. T., Chin, C. H., Hsu, T. T., Chu, D., and Sun, S. H. (2009) *Cell. Signal.* **21**, 881–891
49. Dernick, G., Gong, L. W., Tabares, L., Alvarez de Toledo, G., and Lindau, M. (2005) *Nat. Methods* **2**, 699–708
50. Orriss, I. R., Knight, G. E., Utting, J. C., Taylor, S. E., Burnstock, G., and Arnett, T. R. (2009) *J. Cell. Physiol.* **220**, 155–162
51. Holz, R. W. (2006) *Cell. Mol. Neurobiol.* **26**, 439–447
52. Plattner, H., Artalejo, A. R., and Neher, E. (1997) *J. Cell Biol.* **139**, 1709–1717
53. Becherer, U., and Rettig, J. (2006) *Cell Tissue Res.* **326**, 393–407
54. Rettig, J., and Neher, E. (2002) *Science* **298**, 781–785
55. Xu, T., Rammner, B., Margittai, M., Artalejo, A. R., Neher, E., and Jahn, R. (1999) *Cell* **99**, 713–722
56. Toonen, R. F., Kochubey, O., de Wit, H., Gulyas-Kovacs, A., Konijnenburg, B., Sørensen, J. B., Klingauf, J., and Verhage, M. (2006) *EMBO J.* **25**, 3725–3737
57. Verhage, M., and Sørensen, J. B. (2008) *Traffic* **9**, 1414–1424
58. Bhaskar, K., Shareef, M. M., Sharma, V. M., Shetty, A. P., Ramamohan, Y., Pant, H. C., Raju, T. R., and Shetty, K. T. (2004) *Neurochem. Int.* **44**, 35–44
59. Rizo, J., and Südhof, T. C. (2002) *Nat. Rev. Neurosci.* **3**, 641–653
60. Voets, T., Toonen, R. F., Brian, E. C., de Wit, H., Moser, T., Rettig, J., Südhof, T. C., Neher, E., and Verhage, M. (2001) *Neuron* **31**, 581–591
61. Yizhar, O., and Ashery, U. (2008) *PloS one* **3**, e2694
62. Neher, E., and Sakaba, T. (2008) *Neuron* **59**, 861–872
63. Dinkelacker, V., Voets, T., Neher, E., and Moser, T. (2000) *J. Neurosci.* **20**, 8377–8383
64. von Rüden, L., and Neher, E. (1993) *Science* **262**, 1061–1065
65. Smith, C., Moser, T., Xu, T., and Neher, E. (1998) *Neuron* **20**, 1243–1253
66. Voets, T. (2000) *Neuron* **28**, 537–545
67. Voets, T., Neher, E., and Moser, T. (1999) *Neuron* **23**, 607–615
68. Sperlágh, B., Heinrich, A., and Csölle, C. (2007) *Purinergic Signal.* **3**, 269–284
69. Borisovska, M., Zhao, Y., Tsytsyura, Y., Glyvuk, N., Takamori, S., Matti, U., Rettig, J., Südhof, T., and Bruns, D. (2005) *EMBO J.* **24**, 2114–2126
70. Gil, A., Gutiérrez, L. M., Carrasco-Serrano, C., Alonso, M. T., Viniegra, S., and Criado, M. (2002) *J. Biol. Chem.* **277**, 9904–9910
71. Han, X., Wang, C. T., Bai, J., Chapman, E. R., and Jackson, M. B. (2004) *Science* **304**, 289–292
72. Gualix, J., Abal, M., Pintor, J., and Miras-Portugal, M. T. (1996) *FEBS Lett.* **391**, 195–198